Bulletin of Mathematical Biology (2008) 70: 89–117
DOI 10.1007/s11538-007-9242-9

ORIGINAL ARTICLE

Modeling the VEGF–Bcl-2–CXCL8 Pathway in Intratumoral Agiogenesis

Harsh V. Jain[a], Jacques E. Nör[b], Trachette L. Jackson[a,*]

[a] *Department of Mathematics, University of Michigan, 525 East University, Ann Arbor, MI 48109, USA*
[b] *Departments of Cariology, Restorative Sciences, and Endontics, University of Michigan, 1011 North University Avenue, Ann Arbor, MI 48109, USA*

Received: 22 November 2006 / Accepted: 31 May 2007 / Published online: 16 August 2007

Abstract Recent experiments show that vascular endothelial growth factor (VEGF) is the crucial mediator of downstream events that ultimately lead to enhanced endothelial cell survival and increased vascular density within many tumors. The newly discovered pathway involves up-regulation of the anti-apoptotic protein Bcl-2, which in turn leads to increased production of interleukin-8 (CXCL8). The VEGF–Bcl-2–CXCL8 pathway suggests new targets for the development of anti-angiogenic strategies including short interfering RNA (siRNA) that silence the CXCL8 gene and small molecule inhibitors of Bcl-2. In this paper, we present and validate a mathematical model designed to predict the effect of the therapeutic blockage of VEGF, CXCL8, and Bcl-2 at different stages of tumor progression. In agreement with experimental observations, the model predicts that curtailing the production of CXCL8 early in development can result in a delay in tumor growth and vascular development; however, it has little effect when applied at late stages of tumor progression. Numerical simulations also show that blocking Bcl-2 up-regulation, either at early stages or after the tumor has fully developed, ensures that both microvascular and tumor cell density stabilize at low values representing growth control. These results provide insight into those aspects of the VEGF–Bcl-2–CXCL8 pathway, which independently and in combination, are crucial mediators of tumor growth and vascular development. Continued quantitative modeling in this direction may have profound implications for the development of novel therapies directed against specific proteins and chemokines to alter tumor progression.

Keywords Mathematical model · Anti-angiogenic therapy · Angiogenesis · Bcl-2 · CXCL8

1. Introduction

The vascularization of solid tumors is an inevitable step in cancer progression (Folkman, 1971), therefore, a more complete understanding of it's mechanisms is essential for the

*Corresponding author.
E-mail address: tjacks@umich.edu (Trachette L. Jackson).

development of novel anti-cancer therapies that inhibit the formation of new blood vessels and combat the disease with minimal consequences for the host. Tumor-induced angiogenesis is a highly complex process involving several cellular and subcellular events and although the full picture is still developing, innovative mathematical modeling partnered with experimentation has the potential to facilitate a deeper understanding of the cellular and molecular processes that are integral components of tumor initiation, progression, and treatment.

The classical assays of angiogenesis include the avascular cornea of the rodent eye (Koch et al., 1992; Nör et al., 2001a), the chick chorioallantoic membrane (Nguyen et al., 1994; Ribatti et al., 1996), the hamster cheek pouch (Klintworth, 1973), and the dorsal skin and air sac (Oikawa et al., 1997; Yonekura et al., 1999). Experiments using these assays involve the implantation of tumor cells at a predetermined location within the host. These cells thrive in their new environment and eventually form avascular tumor spheroids. When spheroids reach a critical size (of a few mm in diameter), the constituent cells begin to secrete a wide variety of polypeptide angiogenic factors such as vascular endothelial growth factor (VEGF) (Nör et al., 2001a) in a process controlled by the angiogenic switch. Experimental evidence suggests that this up-regulated expression of angiogenic factors could be in response to deficiencies in oxygen (hypoxia) or glucose (hypoglycemia) (Shweiki et al., 1995). The tumor-derived angiogenic factors diffuse throughout the surrounding tissue, and cause the endothelial cells that line the existing vessels to switch from a previously resting, non-regenerating state to a rapidly dividing group of cells capable of forming new capillary sprouts (Ke et al., 2000) that can grow at the rate of 1 mm per day (Ausprunk and Folkman, 1977). These sprout tips migrate up the chemical gradients of a panel of angiogenic factors (Bernatchez et al., 1999; Terranova et al., 1985) and as they move, new capillaries contiguous with the parent vessels elongate behind them (Pettet et al., 1996a). Neighboring sprouts will eventually fuse together at their tips to form loops (anastomosis), which signal the beginning of circulation of blood. The immature vessels may bud or fuse with other vessels until a complex vascular network develops. Finally, this vessel network penetrates the tumor, providing it with the circulatory system and the supply of nutrients that it requires for growth and progression. These vascular tumors therefore contain blood vessels lined with endothelial cells derived from the animal host.

Recent advances in tissue engineering have allowed for the development of novel approaches to study the in vivo growth of human blood vessels within a mouse model system. Human dermal microvascular endothelial cells (HDMECs) along with oral squamous carcinoma cells are transplanted into severe combined immunodeficient (SCID) mice on biodegradable polymer matrices (Nör et al., 1999, 2001a, 2001b). These matrices function as temporary scaffolds that maintain transplanted cells in a defined space and therefore guide new tissue growth and organization. HDMECs transplanted in this way differentiate into functional human microvessels that anastomose with the mouse vasculature thus generating human tumors vascularized with human microvessels (Nör et al., 2001b). Using such experimental systems, Nör et al. have shown that the pro-angiogenic growth factor VEGF mediates a strong survival signal to microvascular endothelial cells by up-regulating the expression of the anti-apoptotic intracellular protein Bcl-2. They have also demonstrated that over-expression of Bcl-2 in endothelial cells is sufficient to enhance implant microvascular density in immunodeficient mice and to accelerate tumor growth, as compared to controls. An important factor

leading to increased vascularization and enhanced tumor growth is the Bcl-2-mediated up-regulation of CXCL8 (Nör et al., 2001a). CXCL8 is a pro-angiogenic chemokine that simulates both endothelial cell proliferation and migration (Koch et al., 1992; Smith et al., 1994).

Mathematical models of intratumoral angiogenesis have been developed in a number of papers including (Anderson and Chaplain, 1998; Chaplain and Anderson, 1996; Daugulis et al., 2004; Holmes and Sleeman, 2000; Levine et al., 2002, 2001; Nagy, 2004; Plank and Sleeman, 2003; Plank et al., 2004; Tee and DiStefano, 2004). The focus of these studies has mainly been the growth of capillary sprout tips or the initiation of capillary sprout formation from pre-existing vasculature in close proximity of a tumor. In this paper, we aim to develop a quantitative model based on the experiments in Nör et al. (1999, 2001a), wherein the vasculature that develops within the tumor space arises from free human endothelial cells, rather than from pre-existing mouse vessels. Therefore, this model needs to capture the process of microvessel formation from individual endothelial cells which align themselves to form blood vessels, which then anastomose with the existing mouse vasculature. There is also now an abundance of evidence that the VEGF–Bcl-2–CXCL8 pathway is a critical component of the growth and progression of head and neck cancers (Nör et al., 2001a), and a primary objective of our modeling is to better understand the precise role this pathway plays in tumor development and to predict the anti-angiogenic effect of the therapeutic blockade of VEGF, CXCL8, and Bcl-2 at early and late stages of tumor progression.

2. Model development

The mathematical model describes the temporal changes in tumor cell density $N(t)$, HDMEC density $M(t)$, free VEGF concentration $A(t)$, free CXCL8 concentration $L(t)$, and microvessel density $V(t)$. A system of delay differential equations is used to model the evolution of these species with time. A partial model schematic is shown in Fig. 1. The different components of the model equations, beginning with the effects of oxygen and blood-bearing vessels on growing tumor cells, followed by the molecular events associated with the chemical mediators as well as the endothelial cell response to these chemokines, and finally, the microvessel formation rate are discussed below, along with the assumptions that underlie them.

2.1. Tumor cell equation

Following Gammack and Byrne (2001), Ward and King (1999), an empirical model is used to govern tumor cell growth, as given in Eq. (1). The tumor cells proliferate and undergo apoptosis at rates which depend on the local oxygen concentration, C. As oxygen concentration increases to a maximum value (normoxia), the rate of tumor cell proliferation increases until it reaches a maximum value, while the programmed cell death rate decreases to a minimum level. The cell death rate also reflects the limited carrying capacity of the environment.

$$\frac{dN}{dt} = r_1 \frac{C^2}{C_1^2 + C^2} N - r_2 \left(1 - \sigma \frac{C^2}{C_2^2 + C^2}\right) N^2. \tag{1}$$

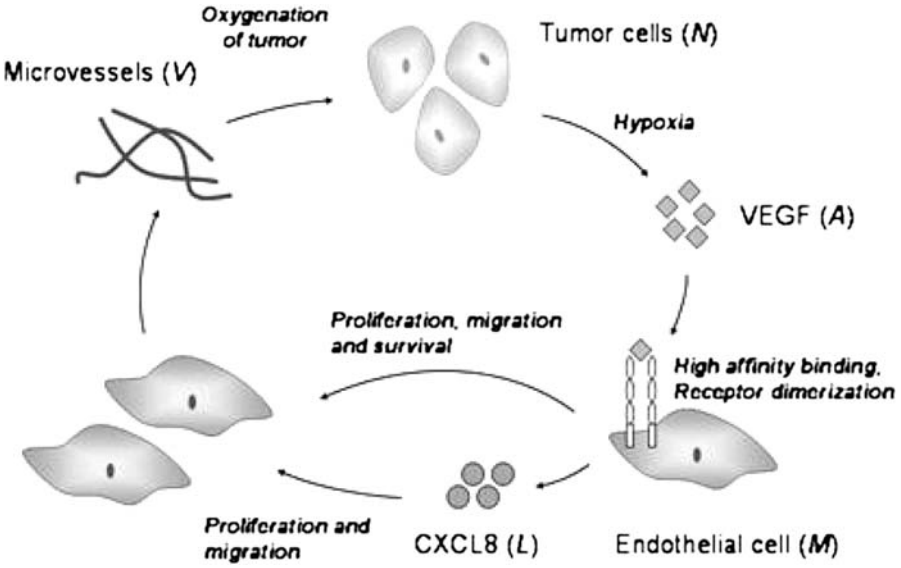

Fig. 1 Partial model schematic. Tumor cells under conditions of hypoxia produce VEGF, which binds to endothelial cells via cell surface receptors and causes receptor dimerization and activation. This elicits a proliferative, chemotactic, and pro-survival response from the endothelial cells, and also results in up-regulation of CXCL8 production by them. CXCL8 in turn induces cell proliferation and chemotaxis. The endothelial cells begin to aggregate and differentiate into microvessels, that eventually fuse with mouse vessels and become blood borne, resulting in oxygenation of the tumor.

To simplify the model, oxygen concentration is treated as a function of blood-bearing vessel density, i.e. oxygen is supplied to implant by the microvessels that have blood flow established in them. The exact form relating the oxygen density C and microvessel density V is taken from Nagy (2004), and is given in Eq. (2).

$$C = C(V) = C_m \frac{V_0 + V}{k + V_0 + V}. \tag{2}$$

Here, C_m is the maximum oxygen concentration, under normoxia (20% oxygen Gammack and Byrne, 2001). Because mouse vessels surround the scaffold, and some oxygen may diffuse through to the tumor cells from these, a fixed minimum vessel density V_0 is assumed in the region of the implant. Most of the parameters associated with Eq. (1) are taken from Gammack and Byrne (2001). Setting the maximum carrying capacity of the environment to be 2.83×10^5 cells per mm^3 (Baxter and Jain, 1991) gives a lower bound for the tumor cell death rate r_2.

2.2. VEGF uptake and binding

VEGF is a 45 kDa homodimeric glycoprotein (Ferrara, 1999) that acts as a potent mitogenic chemokine for endothelial cells (Ferrara, 1999; Ferrara et al., 2003; Leung et al., 1989), and has been shown to inhibit cell apoptosis (Spyridopoulos et al., 1997;

Nör et al., 1999). In vivo it induces angiogenesis and enhances vascular permeability (Kim et al., 1993; Dvorak et al., 1995). Its biological effects are mediated by two receptor tyrosine kinases (RTKs), VEGFR-1 (*flt-1*) and VEGFR-2 (*KDR/flk-1*) (Ferrara et al., 2003). Activation of VEGF RTKs occurs through ligand binding, which facilitates receptor dimerization and autophosphorylation of tyrosine residues in the cytoplasmic portion. The phosphotyrosine residues either enhance receptor catalytic activity or provide docking sites for downstream signaling proteins (McMahon, 2000). However, the in vivo function of VEGFR-1 remains elusive, and it is believed to act mainly as a decoy receptor (Siemeister et al., 1998; Pradeep et al., 2005; Gille et al., 2001). Therefore, VEGFR-2 is the endothelial cell surface receptor of choice for VEGF in this model.

To date, there have been a handful of continuous angiogenesis models that explicitly incorporate VEGF-mediated proliferation of endothelial cells (Holmes and Sleeman, 2000; Levine et al., 2001, 2002; Plank and Sleeman, 2003; Plank et al., 2004; Tee and DiStefano, 2004). The most detailed studies are those in Levine et al. (2001, 2002) where models for the interaction of angiogenic growth factors such as VEGF with growth factor receptors on the surface of endothelial cells are presented. Specifically, in Levine et al. (2001) it is assumed that one molecule of VEGF binds to a receptor (VEGFR) on an endothelial cell surface to produce an intermediate complex. This complex is considered to be an activated state of the receptor that results in the production and secretion of a proteolytic enzyme and a modified intermediate receptor. The intermediate receptor is subsequently removed from the cell surface after which it may be recycled to form the original receptor or a new one is synthesized and moves to the cell surface. Michaelis–Menten kinetics are assumed for this standard catalytic reaction where receptors at the surface of the cell function the same way an enzyme functions in classical enzymatic catalysis. In Levine et al. (2002), the fact that a single molecule of VEGF signals a cascade of intracellular events that results in the production of several (perhaps hundreds) of molecules of proteolytic enzymes is addressed. There is one main issue with this mechanism as it pertains to the VEGF pathway studied here: it does not take into account that receptor dimerization must occur in order to initiate the downstream pathways that lead to CXCL8 synthesis and increased survival.

Therefore, a primary goal of this modeling framework is to accurately describe VEGF dimerization and cellular uptake. This is an important addition to any mathematical representation of VEGF's role in tumor-induced angiogenesis because only modeling with this level of detail will allow for accurate predictions of the therapeutic blockage of VEGFR2.

Following the general approach of Levine et al. (2000), the law of mass action can be used to derive the system of Eqs. (3–6) that describe VEGF uptake by its receptors. Upper case letters represent chemical concentrations, so that A is free VEGF concentration, R_a is VEGFR-2 density, C_a is density of the complex formed when VEGF binds a single molecule of VEGFR-2, and D_a is density of the complex formed when VEGF binds two receptor molecules. Since in experimental assays, the weights of chemokines are often measured in picograms or nanograms, and the length scale of the experiments modeled here is of the order of a few millimeters, the units of concentration have been chosen as pg per mm^3. This introduces scaling factors η_i^a that represent ratios of the weights of the different molecules involved in the reaction. Conservation of total receptor numbers is ensured by setting the sum of the free and bound receptor densities equal to the product

of the average VEGFR2 density per endothelial cell and the endothelial cell density.

$$\frac{dA}{dt} = -2\eta_1^a k_{f1}^a A R_a + \eta_2^a k_{r1}^a C_a - \lambda_a A + r_3 N\left(1 + \tanh\left(\frac{V_{\text{char}} - (V + V_0)}{\epsilon}\right)\right), \tag{3}$$

$$\frac{dR_a}{dt} = -2k_{f1}^a A R_a + \eta_3^a k_{r1}^a C_a - k_{f2}^a C_a R_a + 2\eta_4^a k_{r2}^a D_a + 2\eta_4^v k_p^a D_a, \tag{4}$$

$$\frac{dC_a}{dt} = 2\eta_5^a k_{f1}^a A R_a - k_{r1}^a C_a - \eta_5^a k_{f2}^a C_a R_a + 2\eta_6^a k_{r2}^a D_a, \tag{5}$$

$$\frac{dD_a}{dt} = \eta_7^a k_{f2}^a C_a R_a - 2k_{r2}^a D_a - k_p^a D_a, \tag{6}$$

where

k_{f1}^a is an association rate constant and has units (VEGF concentration)$^{-1}$ (time)$^{-1}$,
k_{r1}^a is a dissociation rate constant and has units (time)$^{-1}$,
k_{f2}^a is an association rate constant and has units (Complex C_a concentration)$^{-1}$ (time)$^{-1}$,
k_{r2}^a is a dissociation rate constant and has units (time)$^{-1}$,
k_p^a is the rate of receptor internalization/recycling and has units (time)$^{-1}$.

Also included in Eq. (3) is the rate of decay λ_a of VEGF in tissue. Further, VEGF is produced by tumor cells under conditions of hypoxia (Shweiki et al., 1995), which occurs when the density of the microvessels is very low. Specifically, the production of VEGF is 'switched on' when the microvessel density falls below a threshold level V_{char}, and 'switched off' when the density exceeds this value. It should be noted that this angiogenic switch causes the microvessel density to stabilize at a maximum level, at around V_{char}. Thus, a production term is added in Eq. (3) governing free VEGF concentration, following (Pettet et al., 1996a).

The multiplicative factor of 2 in some of the equations accounts for the possibility that there may be two ways for that reaction step to proceed. For example, in Eq. (3), there are two ways for a VEGF dimer molecule to bind to a single receptor, since there are two binding sites on the VEGF molecule. The parameter values for VEGF binding dynamics are taken from studies on vascular endothelial cells from the human colon. The values for the rate constants $k_{f1}^a = 1.6232$ pg per mm^3 of VEGF per day and $k_{r1}^a = 40.3025$ per day are obtained from Mac Gabhann and Popel (2004), Wang et al. (2002). Due to a lack of experimental data, the values for k_{f2}^a and k_{r2}^a are difficult to estimate. We justify our choice of their values based on fact that VEGF binding induces receptor aggregation; therefore, it is reasonable to assume that the rate of formation of a dimerized receptor-ligand complex (k_{f2}^a) is greater than the rate of formation of a monomer receptor-ligand complex (k_{f1}^a). Further, because the dimerized complex D_a is the signaling form of the receptor, it is reasonable to assume that D_a is more stable than the monomer complex C_a, i.e. k_{r2}^a is taken to be less than k_{r1}^a. It takes on average, 90 minutes for the receptor-ligand complexes to be internalized and the receptors to be re-released out of the cell (Wang et al., 2002), which gives a value for k_p^a. The average receptor density per cell R_t^a is taken to be 230,000 (Mac Gabhann and Popel, 2004). The tissue half-life of VEGF is about 64 minutes (Serini et al., 2003). For a complete list of parameter values, refer to Table B.1.

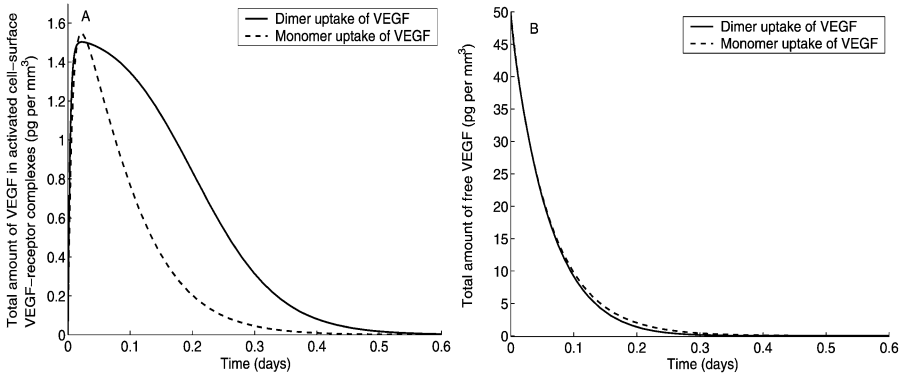

Fig. 2 Dimeric vs. monomeric models of VEGF uptake by endothelial cell surface receptor VEGFR2 result in different solution profiles. A, Amount of VEGF bound in activated VEGF-receptor complexes for the two kinds of uptake have significantly different temporal profiles in experiments with low cell density to initial VEGF concentration ratios. B, Free VEGF concentrations have very similar profiles in such experiments.

2.2.1. Dimer vs. monomer model for VEGF uptake

Typically, in vitro experiments such as those used in this paper for parameter estimation are low cell density experiments (see Sections 2.3–2.5, and Appendix B). Here, low cell density implies low receptor density to VEGF concentration ratio. In these cases, choosing monomeric vs. dimeric uptake and binding of VEGF produces different results. To test the importance of the distinction between these two models, a low cell density (200 cells per mm^3 vs. 50 pg of VEGF per mm^3) numerical experiment is simulated. These numbers correspond to the initial cell concentrations in the in vitro experiments in Nör et al. (2001a). Figure 2 shows graphs of density of VEGF bound in activated VEGF-receptor complexes and free VEGF density versus time, for the two kinds of uptake of VEGF. It should be noted that the free VEGF concentrations have very similar profiles in both cases. However, there is a significant difference in the densities of VEGF in activated complexes. Thus, a free VEGF concentration-dependant endothelial cell proliferation rate may not be a valid assumption. In fact, endothelial cells have a proliferative or chemotactic response dependant on the concentration of activated receptor complexes on their surface, and in such low cell density experiments, choosing the correct form of VEGF binding and uptake is essential for accurately capturing these cellular responses.

2.3. CXCL8 uptake

A novel feature of this model is the incorporation of a second potent angiogenic stimulator, CXCL8. CXCL8 is an 8kDa (Maher, 1995) chemokine produced by many cell types including monocytes, T cells, neutrophils, endothelial cells, and epithelial cells (Mukaida, 2003). It has been shown to induce cell migration, and proliferation more so than VEGF for HDMECs (Koch et al., 1992; Smith et al., 1994; Strieter et al., 1992). CXCL8 binds to two distinct membrane bound receptors, CXCR1 (molecular weight 62kDa Samanta et al., 1989) and CXCR2 (molecular weight 60kDa Horuk, 1994), that mediate signal transduction through G proteins (Mukaida, 2003). These

receptors dimerize independently of the presence of the ligand (Trettel et al., 2003; Wilson et al., 2005) and they undergo hetero-dimerization as well (Wilson et al., 2005). For simplicity, CXCR1 and CXCR2 are not distinguished between in the model. Further, there is no conclusive evidence that two CXCL8 molecules are required to internalize this complex. Thus, it is assumed that one molecule of CXCL8 is sufficient to activate its receptors.

As before, the law of mass action can be used to derive the system of Eqs. (7–9) that describe CXCL8 uptake by its receptors. Upper case letters represent chemical concentrations, so that L is free CXCL8 concentration, R_l is CXCL8 receptor density, and C_l is CXCL8-receptor complex density. The choice of units of concentration introduces scaling factors η_i^l that represent ratios of the weights of the different molecules involved in the reaction. Again, conservation of total receptor numbers is ensured by setting the sum of the free and bound receptor densities to the product of the average CXCR1/2 density per endothelial cell and the endothelial cell density.

$$\frac{dL}{dt} = -\eta_1^l k_f^l L R_l + \eta_2^l k_r^l C_l - \lambda_l L + \beta_l M + \beta_a \phi_a M, \tag{7}$$

$$\frac{dR_l}{dt} = -k_f^l L R_l + \eta_3^l k_r^l C_l + \eta_3^l k_p^l C_l, \tag{8}$$

$$\frac{dC_l}{dt} = \eta_4^l k_f^l L R_l - k_r^l C_l - k_p^l C_l, \tag{9}$$

where

$$\phi_a = \phi_a(D_a, M, V) = \frac{D_a}{M + \alpha_1 V} \tag{10}$$

and

k_f^l is the association rate constant and has units (CXCL8 concentration)$^{-1}$ (time)$^{-1}$,

k_r^l is the dissociation rate constant and has units (time)$^{-1}$,

k_p^l is the rate of receptor internalization/recycling and has units (time)$^{-1}$.

A natural decay rate λ_l of CXCL8 in tissue is also included in Eq. (7). Further, it is known that HDMECs maintain a basic concentration of CXCL8, through a background production rate β_l. It's production by the endothelial cells is up-regulated, in response to up-regulation of Bcl-2 by VEGF. Due to its intracellular nature, Bcl-2 concentration is taken to be directly proportional to HDMEC density, and a separate equation for Bcl-2 is not included Instead, it's effects are modeled using activated VEGF-receptor complex concentration per cell, ϕ_a, as defined in Eq. (10). Here, $D_a(t)$ is the overall concentration of activated VEGF-receptor complexes, as given by Eq. (6). This is divided by the total endothelial cell density which includes free cells as well as those cells that have differentiated to form microvessels. Note that vessel cells are capable of binding VEGF, and although they may not necessarily respond by proliferating, we assume that VEGF leads to up-regulated survival in the cells lining immature vessels as well. The parameter α_1 is the number of cells on average per microvessel.

CXCL8 binding dynamics have been studied mostly on human neutrophils and in the absence of data on endothelial cells, some parameter values have been taken from these studies. For example, the equilibrium rate constant $k_D^l = k_r^l / k_f^l$ is taken as 0.8 nM (Holmes et al., 1991), the mean recycle time for CXCL8 receptors is about 60 minutes (Mukaida, 2003), from which k_p^l is determined, and the average receptor density per cell R_t^l is taken to be 31,000 (Holmes et al., 1991). A few parameters were derived from least squares fits to HDMEC vs. time data taken from in vitro experiments. In one set of experiments described in Nör et al. (1999), endothelial cells are cultured in the presence of CXCL8, VEGF and in the control case, without chemokines. Data from the second of these is used to estimate Bcl-2 dependent CXCL8 production rate β_a. The background CXCL8 production rate β_l of endothelial cells is estimated from the control experiment. For a complete list of parameter values, refer to Table B.1.

2.4. Endothelial cell response to VEGF and CXCL8

In contrast to other models which assume that endothelial cell proliferation depends on extra-cellular growth factor concentrations or on monomeric binding of VEGF, our model assumes that HDMEC proliferation and death rates as well as the CXCL8 production rate are directly proportional to the amount of VEGF bound (in dimer form) to receptors on cell surfaces. To our knowledge, this has never before been considered in a mathematical model of tumor-induced angiogenesis or vascular tumor growth. The rate of change of the free HDMEC population is represented in Eq. (11). The units of endothelial cell ($M(t)$) and vessel ($V(t)$) densities are number per mm^3. It should be noted that we have simplified the vascular network into a series of equal length units, and 'a microvessel' is one segment between adjacent branching points that can fit into a cube of side one millimeter.

$$\frac{dM}{dt} = \big(\mu_a \phi_a + \mu_l \phi_l - (\lambda_m - \delta \phi_a)\big) M \left(1 - \frac{M}{M_0 - \alpha_1 V}\right), \tag{11}$$

where

$$\phi_l = \phi_l(C_l, M, V) = \frac{C_l}{M + \alpha_1 V}. \tag{12}$$

The HDMECs are assumed to grow logistically, as the carrying capacity M_0 of this experimental environment is limited. M_0 is estimated to be 17,000 cells per mm^3 from the experiments in Nör et al. (2001a). The endothelial cells lining the microvessels also compete with the free endothelial cells for space and nutrients. This is incorporated into the logistic term by reducing the carrying capacity by the density of endothelial cells lining the microvessels, i.e. $\alpha_1 V$. Note that the vessel density is bounded near a level at which the tumor is nourished by enough vessels to be in normoxia, so $\alpha_1 V$ does not exceed 2,000 cells per mm^3. Since the value of M_0 is far greater than that of $\alpha_1 V$, the effective carrying capacity of the environment, $M_0 - \alpha_1 V$, will never become negative.

The first two terms in Eq. (11) give endothelial cell proliferation rates. While there is no explicit experimental evidence that effects of VEGF and CXCL8 on HDMECs are additive, we believe that this is a reasonable assumption in the absence of data to the contrary. Our rationale for making this choice stems from the knowledge that VEGF is a potent mitogenic and chemokinetic factor for endothelial cells, and that CXCL8 alone

is also capable of inducing cell proliferation and differentiation (Nör et al., 1999). These cellular responses are a result of the activation of cell surface receptors for these two chemokines. Hence, the proliferation rate of HDMECs due to VEGF is taken to be proportional to the average density of activated VEGF-receptor complexes per cell (ϕ_a, as defined in Eq. (10)). Likewise, the proliferation rate of HDMECs due to CXCL8 is taken as proportional to the average density of activated CXCL8-receptor complexes per cell (ϕ_l, as defined in Eq. (12)). It should be noted that vessel cells also have receptors for CXCL8, so its uptake by these cells is included. This reduces the amount of free CXCL8 available to free endothelial cells. Here $C_l(t)$ is the overall concentration of activated CXCL8-receptor complexes, as given by Eq. (9).

Moving now to the third term in Eq. (11), λ_m gives the natural death rate of endothelial cells. The anti-apoptotic effect of the intracellular protein Bcl-2, whose expression is up-regulated in presence of VEGF, is also incorporated here. As mentioned in the previous section, the effects of Bcl-2 are modelled using activated VEGF-receptor complex concentrations and the natural death rate λ_m of HDMECs is reduced by a factor dependant on ϕ_a. Conservation of receptors ensures that the total number of VEGF receptors per cell R_t^a is fixed; this also ensures that the densities of VEGF-receptor complexes per mm^3—C_a and D_a—are bounded above by $R_t^a \times M_0$, and that the density of activated VEGF-receptor complexes per cell ϕ_a is bounded above by R_t^a. Since the Bcl-2 dependent death rate of HDMECs cannot be negative, this gives a natural upper bound (λ_m / R_t^a) for the multiplicative factor δ.

Parameters associated with the endothelial cell equation were chosen from values given in the literature, or derived from best fits to in vitro experimental data. In order to perform these fits, the model is first reduced to represent the in vitro system, then a least squares fit of the modified model to the HDMEC vs. time experimental data is performed. In one set of experiments described in Nör et al. (1999), endothelial cells are cultured in the presence of CXCL8, VEGF and in the control case, without chemokines. Data from the first of these is used to estimate CXCL8 dependant HDMEC proliferation rate μ_l, and rate association constant k_f^l. The second set of experiments yield VEGF dependant HDMEC proliferation rate μ_a, and Bcl-2 dependent death rate reduction factor δ.

2.5. Microvessel formation and degradation

As endothelial cells grow in number, they begin to come together and arrange themselves into microvessels during the process of vascular inclusion. Previous models of angiogenesis have looked at microvessel formation in response to growth factor stimuli from a hypoxic tumor including (Anderson and Chaplain, 1998; Chaplain and Anderson, 1996; Nagy, 2004) or in the context of wound healing Pettet et al. (1996a, 1996b). In their model of angiogenesis in wound healing, Pettet et al. (1996a, 1996b) assume an initial condition of preformed capillary tips, that migrate towards the hypoxic center of a wound, pulling behind them blood vessels contiguous with parent vessels. Anderson and Chaplain (1998) begin with a tumor source located at a certain distance from parent vessels. It is assumed that sprout tips have already formed along this vessel and these tips migrate toward the tumor in response to growth factors. Both papers address blood vessel formation that results from pre-existing vasculature, while here we need to model the process of microvessel formation via alignment and differentiation of individual endothelial cells. Nagy (2004) incorporates the formation of new vessels that arise from (free) activated

vascular endothelial cells at a constant rate, independent of growth factor concentration. In our model, however, growth factor concentration is taken into account during vessel formation. Further in Nagy (2004), the vessel degradation rate depends on limitations of space and growth factor availability. Here, the limitations of resources have already been included in the logistic term of Eq. (11).

Equation (13) gives the rate of change of microvessel density. VEGF and CXCL8 are both believed to be strong chemoattractants for the HDMECs, so that the cells align and form microvessels at a rate dependant on the activated receptor density functions ϕ_a and ϕ_l, which appear in the first two terms of Eq. (13). This process of vascular inclusion results in a corresponding decrease in the free endothelial cell density. Thus, a vascular inclusion term is subtracted from the endothelial cell equation and Eq. (11) changes to Eq. (14). Here, α_1 is the average number of cells per microvessel. Vessel maturation is not part of this model. Therefore, when cells lining an immature vessel die, it is assumed to become dysfunctional at rate, α_4. In addition, the microvessel degradation rate includes a term to study the anti-apoptotic effect of Bcl-2. Like the death term in the free endothelial cell Eq. (14), up-regulated levels of Bcl-2, i.e., high numbers of active VEGF-receptor complexes on the cells lining the microvessels reduce their death rate. The density of cells that have rolled up to form microvessels is given by $\alpha_1 V$.

Since the ODE model presented here is independent of space, chemotaxis is not included explicitly. Budding and anastomoses have also not been included in this model, since this would present further unknown parameters, and there does not appear to be any conclusive evidence that these processes significantly affect microvessel densities within the implant.

$$\frac{dV}{dt} = (\alpha_2\phi_a + \alpha_3\phi_l)M_\tau - \alpha_4(\lambda_m - \delta\phi_a)\alpha_1 V, \tag{13}$$

$$\frac{dM}{dt} = \big(\mu_a\phi_a + \mu_l\phi_l - (\lambda_m - \delta\phi_a)\big)M\left(1 - \frac{M}{M_0 - \alpha_1 V}\right) - \alpha_1(\alpha_2\phi_a + \alpha_3\phi_l)M_\tau. \tag{14}$$

A delay τ is incorporated in the vessel formation rate, to account for experimentally observed time delay between an endothelial cell receiving a signal in the form of activated cell surface receptors, and differentiating to form mature, blood-bearing microvessels. The principle steps leading to the formation of microvessels via the processes of vasculogenesis and angiogenesis are described in Patan (2000). Briefly, the cells, upon receiving a chemical stimulus, may proliferate or migrate towards this signal in a process known as chemotaxis. As the cells begin to align together, they abandon their invasive phenotype, and begin forming cell–cell adhesions and reassociate with the extracellular matrix, via cell surface molecules such as integrins. This is followed by stretching and thinning of the cells, and their alignment in bipolar mode. The next step is vacuole and lumen formation. As more and more cells come together intracellular vacuoles fuse, and the lumens enlarge to generate tubular structures. Finally, these structures are stabilized, by specialized cells such as pericytes and smooth muscle cells that assist in basement membrane formation, to produce a microvessel capable of carrying blood. The steps involved in capillary formation detailed above are accounted for by the inclusion of a delay in vessel formation. Time delays in vessel formation/regression terms have been used previously in Daugulis et al. (2004) wherein ODE models are presented for tumor induced angiogenesis.

In the experiments in Nör et al. (2001a), the first vessels in the scaffold are seen only about 5 days after implantation, indicating that the value for the delay τ is 5. It should be noted that a delay of zero days implies that endothelial cells differentiate into vessels as soon as any chemical stimulus is provided, in essence completing all the steps that must precede the differentiation instantaneously. Further, the first of these vessels would already be blood bearing, while blood flow can only be established once the vasculature within the implant has had time to anastomose with neighboring mouse vessels.

Experiments described in Dong et al. (2007) are set up to investigate the apoptotic requirement of endothelial cells for microvessel disruption. The control experiments herein are used to estimate three parameters, viz. the VEGF and CXCL8 dependent vessel formation rates, and Bcl-2 dependent loss of functional vessels rate.

3. Results

3.1. Vascular tumor growth

All numerical simulations of the model described in the previous section were carried out using RADAU IIA methods adapted to solve delay differential equations, as implemented by the numerical package RADAR5 Version 2.1 (Guglielmi and Hairer, 2001). Two key indicators of tumor development were studied in particular—maximal steady state values of tumor cell and vessel densities, and the time taken to reach these.

First, a series of numerical simulations are performed to illustrate tumor growth dynamics in the absence of anti-angiogenic or any other anti-cancer therapies. Two parameters were varied: tumor cell sensitivity to oxygen deprivation, that is the rate at which cells become necrotic in a low oxygen environment (r_2), and tumor cell ability to produce VEGF which captures the variation in the production of VEGF by different tumor cell lines (r_3). The results are summarized below.

With parameters at their baseline values, the tumor cell density reaches it's maximum level (1.149×10^4 cells per mm^3) about 28 days after implantation (Fig. 3A). The first blood-bearing vessels are seen 5 days after implantation, reaching their steady state of about 53 vessels per mm^3, 19 days later (Fig. 3B). During the first five days, the scaffold is hypoxic and a transient decrease in tumor cell density is observed that may be attributed to necrosis (Fig. 3A, inset).

Next, a sensitivity analysis is carried out on the tumor cell oxygen sensitivity parameter (r_2). Numerical simulations indicate that maximal tumor cell density reached is exponentially related to r_2. As r_2 is varied from 10% to 150% of its control value, the maximal tumor cell densities decrease from 11.58×10^4 cells per mm^3 to 0.76×10^4 cells per mm^3—a change of about 93%. However, the maximal vascular densities reached vary only from 54 to 52 vessels per mm^3—change of only 4%—and appear to be linearly related to the oxygen sensitivity parameter. These cell and vessel densities are normalized by their respective maximum values, and plotted vs. r_2 (Fig. 4A). For the same variation in the oxygen sensitivity parameter, the time taken by the tumor cells to reach maximal density increases from 18 to 62 days, and the time taken to reach maximum vascular densities increases from 12 to 57 days (Fig. 4B), i.e. tumor growth and vascular development occur at a similar pace, and seem to vary exponentially with tumor cell sensitivity to oxygen deprivation. These results can be explained by the fact that a delay in tumor

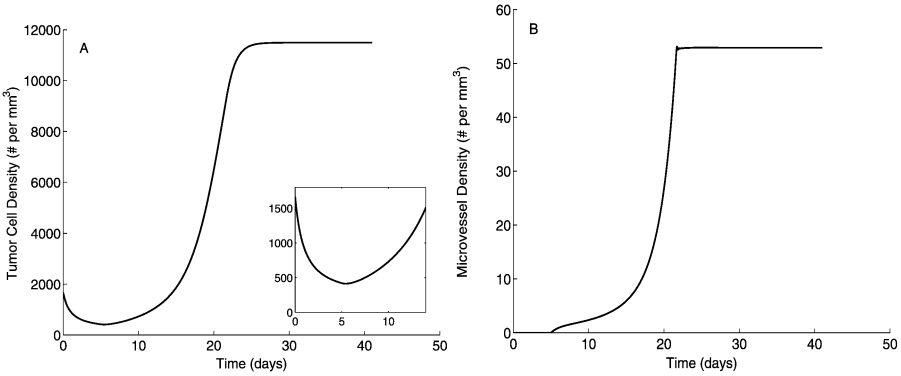

Fig. 3 Vascular tumor growth in the absence of therapeutic intervention. A, Tumor cell density reaches its steady state of 1.149×10^4 cells per mm^3 about 28 days post implantation. A transient decrease in tumor cell density is observed due to hypoxic conditions within the implant for the first week (inset). B, Blood borne vessels are first seen 5 days after implantation, and reach their maximal level of 53 vessels per mm^3 about 24 days post implantation.

cell growth results in a delay in VEGF concentration reaching its maximum level, which correspondingly causes a delay in vasculature development. However, tumor cells are still producing VEGF at the same rate, and while the VEGF concentration falls with a reduction in tumor cell density, the change is not large enough to significantly alter the steady state reached by the vasculature. Thus, tumor cells that are more sensitive to local oxygen concentrations give rise to tumors that have very low tumor cell density, but are still highly vascularized. On the other hand, tumor cells with greater resistance to hypoxic conditions produce highly vascularized tumors with very high tumor cell densities.

Finally, a sensitivity analysis is carried out on the rate of VEGF production (r_3). This captures the variation in production of VEGF by different types of cancer cells and can also describe therapeutic intervention associated with administering small molecule inhibitors of VEGF. As expected, the numerical simulations predict that decreasing VEGF production rate delays tumor growth and vascular development. As VEGF production by tumor cells is decreased, the time taken by the tumor cells to reach maximum densities increases, from 17 days to 61 days, and time taken by the vessels to reach maximum densities increases from 13 to 57 days (Fig. 4D). The relationship between VEGF production rate and both these times appears to be exponential. On the other hand, maximum tumor cell densities reached decrease by only 1%, from 1.157×10^4 to 1.144×10^4 per mm^3, and maximum vessel densities reached decrease by about 4% from 54 to 52 per mm^3, for the same variation in r_3. These cell and vessel densities are normalized by their respective maximum values, and plotted versus r_3 (Fig. 4C). Thus, decreasing VEGF production rate has a far greater impact on the time taken to reach maximal cell and vessel densities than on their actual maximum values. This indicates that the fall in VEGF production is enough to significantly retard vessel formation, but not enough to affect the steady state reached by the vessel density. Since the other parameters including tumor cell growth and necrosis rates are kept fixed, the tumor cells are able to grow to roughly the same steady states.

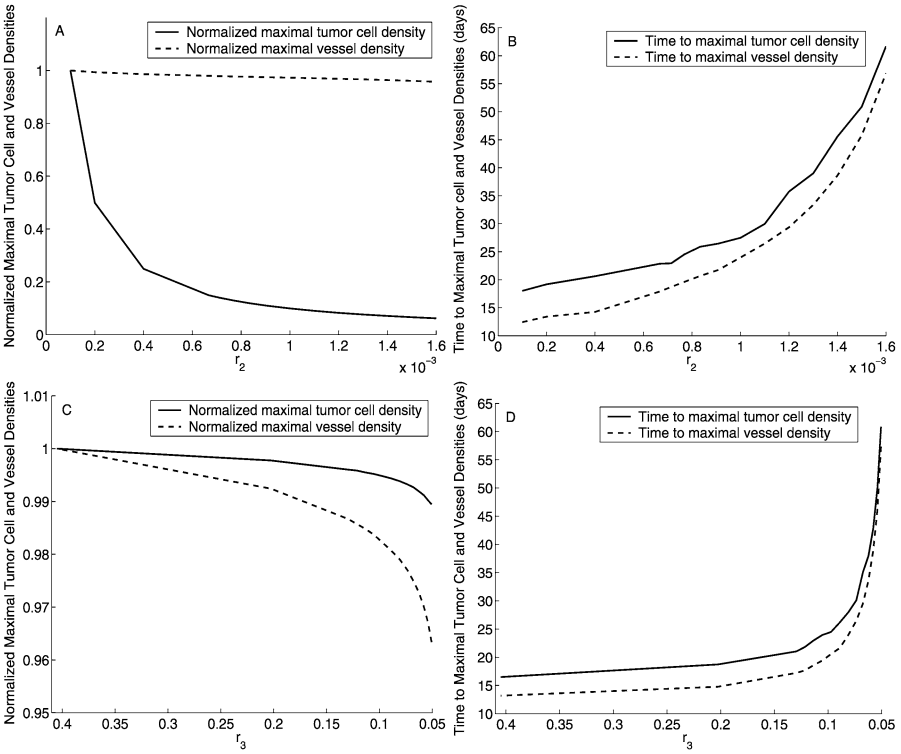

Fig. 4 Tumor cells with high oxygen deprivation sensitivity give rise to highly vascularized tumors with low tumor cell densities. Decreasing tumor cell VEGF production rate delays tumor growth significantly. A, B, Effect of increasing tumor cell oxygen deprivation sensitivity from 10% to 150% of its baseline value is simulated. Numerical results predict a 93% reduction in maximal tumor cell density. The corresponding reduction in maximal vessel density is only 4% (A). The time taken to reach maximal tumor cell density increases by a factor of 3.5, while that to reach maximal vessel density increases by a factor of 4.8 (B). C, D, Effect of decreasing VEGF production rate from 500% to 62.5% of its baseline value is simulated. Numerical results predict a reduction of only 1% in maximal tumor cell density and a reduction of only 4% in maximal vessel density (C). However, the corresponding increase in time taken to reach maximal tumor cell and vessel density is as much as 3.6 and 4.4 fold respectively (D).

3.2. Anti-angiogenic therapy targeted at the VEGF–BCL-2–CXCL8l pathway

The main focus of this paper is to investigate the importance of the downstream effect of the VEGF–Bcl-2–CXCL8 pathway in tumor progression. The pathway suggests two targets for the development of anti-angiogenic therapies: inhibiting the production of CXCL8 by HDMECs and blocking the VEGF mediated up-regulation of Bcl-2 by HDMECs. Numerical simulations of both these cases are carried out keeping all previously introduced parameters fixed at their estimated pre-treatment values. The results are presented and discussed below.

3.2.1. Anti CXCL8 therapy

The effect of inhibiting the production of CXCL8 from the first day of implantation is investigated. Experimental data is taken from Nör et al. (2001a), where polyclonal antihuman CXCL8 antibody was delivered locally, by incorporation into the scaffolds implanted in the SCID mice. The mice were then sacrificed after 21 days and vascular densities noted. The vasculature in treated tumors reached a density of around 20 vessels per mm^3 after 21 days, as opposed to a tumor that was allowed to grow without the application of any anti-cancer therapy, in which the density was double this value, at around 42 vessels per mm^3 after the same length of time (Fig. 5C). The anti-CXCL8 antibody binds to free CXCL8, effectively reducing the bio-availability of free CXCL8 for endothelial cells. In modeling terms, this can be thought of as a reduction in the production rate of CXCL8,

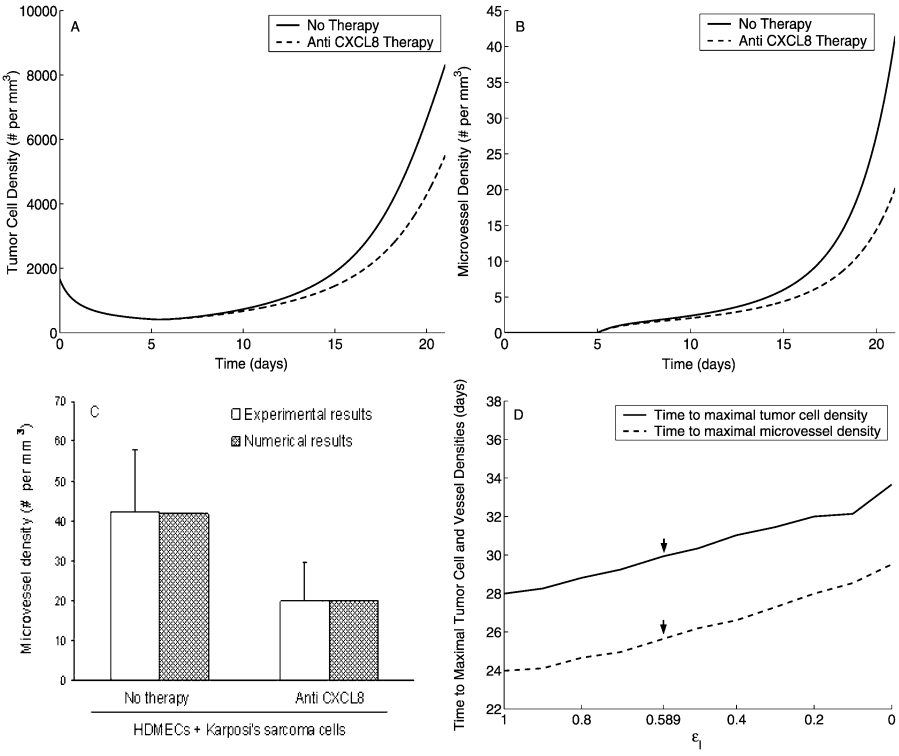

Fig. 5 Anti CXCL8 therapy applied on the first day of implantation delays both tumor growth and vascular development. A, B, Numerical simulations of anti CXCL8 therapy applied from the first day, predict that after 21 days, the tumor cell density is about 32% lower than its value in the case when no therapy is applied (A). Likewise, the vessel density in the anti CXCL8 case is 50% lower than its value in the case with no therapy applied (B). C, Comparison of experimental and numerical predictions of microvessel densities (vessels per mm^3) after 21 days of exposure to anti CXCL8 therapy. Experimental data taken from Nör et al. (2001a), where sponges seeded with HDMECs and Kaposi's sarcoma cells were implanted in severe combined immunodeficient mice. Polyclonal antihuman CXCL8 antibody was delivered by incorporation into scaffolds implanted in the mice. D, Time to both maximal tumor cell and vessel densities increases by about 6 days for a 100% efficacious therapy level, as opposed to the no therapy case. $\epsilon_l = 0.589$ corresponds to the in vivo therapy in Nör et al. (2001a).

which would mean lower levels of free CXCL8 available to the endothelial cells. Thus, anti CXCL8 therapy can be modeled via a parameter ϵ_l, which is a measure of therapy efficacy, and multiplies the CXCL8 production term in Eq. (7). It varies from 1 (no therapy applied) to 0 (100% efficacious therapy). Inclusion of anti-CXCL8 therapy changes Eq. (7) as follows.

$$\frac{dL}{dt} = -\eta_1^l k_f^l L R_l + \eta_2^l k_r^l C_l - \lambda_l L + \epsilon_l(\beta_l M + \beta_a \phi_a M). \tag{15}$$

Numerical simulations show that as ϵ_l is varied from 1 to 0, the vessel density after 21 days changes from 42 to 12 vessels per mm^3. Comparison with experimental results allows us to calculate that the in vivo therapy in Nör et al. (2001a) has an efficacy level between 20% ($\epsilon_l = 0.8$) and 100% ($\epsilon_l = 0$) (Fig. 5C, $\epsilon_l = 0.589$, efficacy level of 41.1%). This range of values for ϵ_l is obtained from experimental error bars. The tumor cell density in a tumor growing without treatment is 48% higher than in a tumor treated with the above level of anti CXCL8 therapy after in 21 days (Fig. 5A). Correspondingly, the treated tumor is nourished by only half the vasculature in a non-treated tumor, at this point of time (Fig. 5B).

It is also important to determine how varying CXCL8 therapy levels affects the delay in tumor development. As can be seen from Fig. 5D, time taken to reach maximal tumor cell and vessel densities appears to vary linearly with ϵ_l. A 100 % efficacious therapy level, corresponding to $\epsilon_l = 0$ introduces a delay of 6 days in tumor development, while the delay is only 2 days corresponding to the in vivo therapy in Nör et al. (2001a) ($\epsilon_l = 0.589$). Note that in Fig. 5D, ϵ_l varies from 1 to 0 on the abscissa, which should be interpreted as level of therapy increasing from 0 to 100%. Thus, anti CXCL8 therapy delays tumor growth, but the delay is not very large. Further, the maximal levels of tumor cell and vessel densities remain unaffected upon application of therapy. This can be explained by observing that CXCL8 is not directly related to enhanced endothelial cell survival, it induces cell proliferation and migration. But these functions are also performed by VEGF which in addition exerts a pro-survival effect on the endothelial cells though up-regulation of Bcl-2. So reducing CXCL8 levels can be expected to produce a delay in vascular development, which correspondingly delays tumor cell growth. However, tumor cell VEGF production rate remains unchanged, which explains the relatively small value of the delay, and also accounts for the unchanged maximal vessel density. This in turn means that maximal tumor cell density remains unchanged, since it is a function of the blood-bearing vessel density.

3.2.2. Anti Bcl-2 therapy

Numerical simulations of the clinically interesting situation corresponding to intercepting the effect of VEGF on Bcl-2 levels within HDMECs both in vitro and in vivo were performed. In Karl et al. (2005) in vitro, capillary sprouting assays with HDMECs exposed to 50 ng/ml of VEGF are compared with HDMECs cultured in the presence of 50 ng/ml VEGF and exposed to anti Bcl-2 therapy starting on day 5, in the form of a small molecule inhibitor BL193. The model equations are modified to simulate the in vitro experiments. Notably, there are no tumor cells present and free VEGF concentration is held fixed at 50 ng/ml. Constitutive CXCL8 production rate by endothelial cells and environmental carrying capacity for endothelial cells are re-evaluated from the control (no

therapy) simulations. To model the effect of anti Bcl-2 therapy, a parameter ϵ_a is introduced as a measure of the level of blockage of Bcl-2 up-regulation by BL193. This affects the cell death terms in the free HDMEC and vessel equations, and CXCL8 up-regulation by HDMECs in the presence of VEGF. Equations (7), (13) and (14) change as follows.

$$\frac{dL}{dt} = -\eta_1^l k_f^l L R_l + \eta_2^l k_r^l C_l - \lambda_l L + \beta_l M + \epsilon_a \beta_a \phi_a M, \tag{16}$$

$$\frac{dV}{dt} = (\alpha_2 \phi_a + \alpha_3 \phi_l) M - \alpha_4 (\lambda_m - \epsilon_a \delta \phi_a) \alpha_1 V, \tag{17}$$

$$\frac{dM}{dt} = \left(\mu_a \phi_a + \mu_l \phi_l - (\lambda_m - \epsilon_a \delta \phi_a)\right) M \left(1 - \frac{M}{M_0 - \alpha_1 V}\right) - \alpha_1 (\alpha_2 \phi_a + \alpha_3 \phi_l) M. \tag{18}$$

The level of Bcl-2 up-regulation blockage ϵ_a may be varied between 1 (no therapy) and 0 (complete blockage of Bcl-2 up-regulation), and the results compared with experimental outcomes. Note that setting $\epsilon_a = 0$ forces Bcl-2 to remain at its normal, constitutive levels and ensures that production of CXCL8 is not up-regulated. It is observed that the model provides a good fit to the no therapy case (Fig. 6C). The numerical and experimentally observed vessel densities are seen to be in good agreement when the blockage level of Bcl-2 up-regulation by VEGF is between 85% and 100% (Fig. 6D, complete blockage of Bcl-2 up-regulation).

Next, the effect of small molecule inhibition of Bcl-2 may be numerically investigated in vivo. The model predicts that after 21 days, when Bcl-2 up-regulation is blocked completely ($\epsilon_a = 0$), post-therapy tumor cell and vasculature densities drop to levels 27.5% and 14%, respectively, of their values when no therapy is applied, (Figs. 6A, B). Further, the maximal tumor cell and vessel densities may also be plotted as the level of blocking of Bcl-2 up-regulation is varied (Fig. 6E). Interestingly, there appears to be a minimum level of blockage of Bcl-2 up-regulation by VEGF required for the therapy to be effective. For $\epsilon_a < 0.4$, anti Bcl-2 therapy has comparatively little effect on tumor development, and maximal tumor cell and vessel densities do not change appreciably. With a reduction in Bcl-2 up-regulation levels, the endothelial cell death rate increases, and CXCL8 production by endothelial cells decreases, but these effects are balanced out to some extent by an unchanged tumor cell VEGF production rate. However, as ϵ_a is reduced further, the endothelial cell apoptosis rate becomes very large, and consequently, maximal vessel densities begin to fall drastically. This causes a drop in maximal tumor cell densities as well, since there are fewer blood-bearing vessels supplying nutrients and oxygen to the tumor. Eventually, corresponding to in vitro therapy levels ($\epsilon_a = 0$), tumor cell density stabilizes at 68% and vessel density stabilizes at 41% of their values in the no therapy case. This sensitivity of the tumor to anti Bcl-2 therapy levels is also apparent from the graphs of time taken to reach maximal cell and vessel densities vs. therapy level (Fig. 6F). For $\epsilon_a < 0.4$, the delay in vessel and tumor development increases fairly slowly, with an increase in therapy level. Near $\epsilon_a = 0.4$, the rates of change of both these times are maximum, and for higher therapy levels, these rates seem to level out, but are still high. Overall, it takes about 30 days longer for the tumor to develop when Bcl-2 up-regulation is completely blocked. These results underscore the use of this model as a predictive tool to guide in vivo experiments aimed at testing anti Bcl-2 therapies. They suggest that below a certain

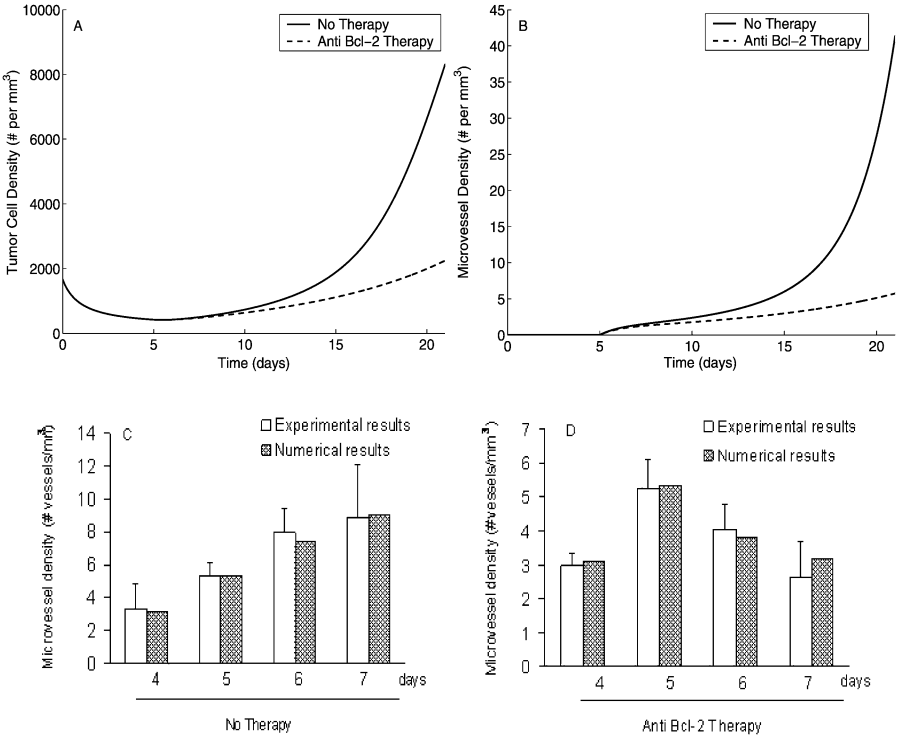

Fig. 6 Anti Bcl-2 therapy is highly effective in controlling tumor growth and vascular development. A, B, Numerical simulations of in vivo anti Bcl-2 therapy corresponding to 100% blockage of Bcl-2 up-regulation by VEGF applied from the first day predict that after 21 days, the tumor cell density is only about 27.5% of its value in the case when no therapy is applied (A). Likewise, the vessel density in the anti Bcl-2 case is about 14% of its value in the case with no therapy applied (B). C, D, Comparison of numerical simulations and experimental results of in vitro capillary sprouting assays with HDMEC exposed either to 50 ng/ml VEGF (A) or 50 ng/ml VEGF and anti Bcl-2 therapy starting on day 5 in the form of 0.5 M of BL193, a small molecule inhibitor of Bcl-2 (D). Experimental data taken from Karl et al. (2005). E, F, Anti Bcl-2 therapy appears to have a major effect only after a minimum level of therapy, corresponding to $\epsilon_a = 0.4$, is provided. Maximal tumor cell density and maximal microvessel density show a drop of 30% and 59% respectively as level of anti Bcl-2 therapy is increased from no therapy to 100% blockage of Bcl-2 up-regulation (E). Time taken to maximal tumor cell density increases by 90% and to maximal vessel density increases by 112% for this range of therapy (F).

threshold, anti Bcl-2 therapy elicits little response from the tumor, but as therapy is increased beyond this threshold, the tumor and vascular development is arrested at much lower levels. Thus, anti Bcl-2 therapy is considerably more effective than anti CXCL8 therapy, if given in the right quantities. It should be noted that in Figs. 6E, F, ϵ_a varies from 1 to 0 on the abscissa, which should be interpreted as level of therapy increasing from 0 to 100%.

3.2.3. Treatment of fully-formed tumors

We investigated the effect of various anti-angiogenic therapies applied to a tumor that has been allowed to reach maximal tumor cell and microvessel densities (Figs. 7A, B). The

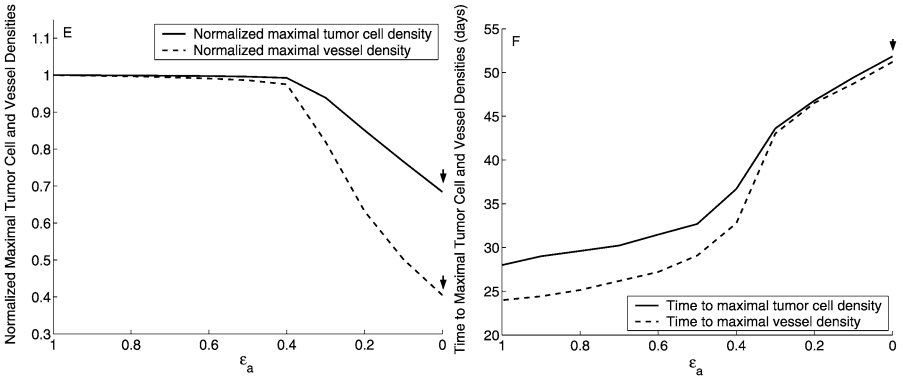

Fig. 6 (*Continued.*)

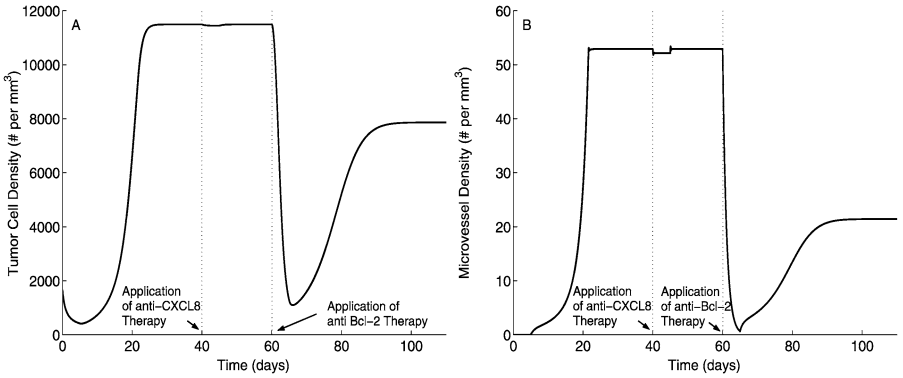

Fig. 7 A fully formed tumor responds to anti Bcl-2 therapy, while anti CXCL8 therapy appears to have little or no impact. A, B, Anti CXCL8 and anti Bcl-2 therapies are applied in turn on a fully developed tumor, and their effects on tumor cell and microvessel density graphed. The anti CXCL8 therapy is applied on the 40th day, and the anti Bcl-2 therapy is applied on the 60th day. It can be seen that while the anti CXCL8 therapy has little affect the tumor cell and microvessel densities, anti Bcl-2 therapy produces a significant drop in both of these.

model predicts that anti CXCL8 treatment has little or no effect on the tumor when applied at this late stage. The vessel density is seen to decrease only slightly, but the tumor cells appear to compensate for this decrease in CXCL8 levels by increasing VEGF production. The vessel density soon returns to its pre-treatment level. However, if the up-regulation of Bcl-2 in HDMECs is blocked, the tumor begins to regress and finally stabilizes at lower cell and vasculature densities. This underscores the importance of enhanced HDMEC survival in the progression of a tumor. Note that in Fig. 7B, a sudden drop in the vessel density is observed when anti Bcl-2 therapy is applied. In actual experiments this drop may be more gradual. In the numerical simulation, at the point of application of the therapy, the Bcl-2 levels in the cells are set to non up-regulated levels while in all probability, it would take some time for these to be achieved in vivo.

4. Effect of the delay τ

An important feature of this model is the inclusion of a delay in the microvessel formation, to account for the various biological steps that precede the differentiation of free endothelial cells into capillaries. We are not the first to use a delay in this way—in Kuang et al. (2004), Kuang et al. use a delay to account for the time it takes activated vascular precursor cells to mature into functional microvessels. Time delays in vessel formation have also been used in angiogenesis models to rationalize empirical observations (Daugulis et al., 2004). Experimental observations allow us to fix this delay at 5 days. Various numerical experiments were carried out to test the stability of steady states of the model revealed that the introduction of the delay did not produce any oscillatory behavior.

To investigate the importance of the delay, the model equations are simulated with $\tau = 0$ representing the non-delay case. In setting the delay to zero, we are making the biologically unreasonable assumptions that the endothelial cells begin to form vessels as soon as they detect any sort of chemical stimulus, and these vessels are also blood bearing immediately. It is observed that tumor cell density stabilizes almost 12 days earlier and vessel density stabilizes almost 10 days earlier than if the delay is fixed at 5 days. In fact, after 21 days, the tumor cell and vessel densities have already reached their maximal levels, and the vessel density is 27% higher than the value observed experimentally in the case when the delay is set to zero (Figs. 8A, B). Thus, the tumor vasculature is developing at a rate that is much faster than what is observed in vivo.

Next, the effect of the length of the delay on time taken to reach maximal tumor and vessel densities is studied. The delay is varied between biologically realistic values of 0.5 days to 10 days. The time taken to maximal tumor cell density increases from 18 days to 34 days—a change of 89%. The time taken to reach maximal vessel density also increases by about 88% from 16 days to 30 days (Fig. 8C). Interestingly, for τ between 0.5 and 3 days, the delay between tumor cell and vessel development is about 2 days, but for τ greater than 4 days, this delay increases to 4 days (Fig. 8D).

5. Discussion

There have been numerous advances in the development of experimental models to study angiogenesis, recasting these in mathematical terms can provide valuable insights into understanding the processes that govern angiogenesis and suggest new methods of treatment of cancers. We set out to explore quantitatively one such experimental model that investigated the importance of the VEGF–Bcl-2–CXCL8 pathway in sustained angiogenesis of a developing tumor. The main goal of this research was to derive a mathematical model of the experiments in Nör et al. (1999, 2001a), in order to better understand those features of the pathway which play the most crucial role in sustaining the growth of a tumor. Further, numerical simulations of the model could be used to suggest new areas for the development of anti-angiogenic therapies targeted at the proteins and chemokines involved in the pathway and to assess their effects on tumor progression. We recognize that this experimental system does not exactly replicate the formation of human tumors in vivo, however this experimental approach has lead to several significant discoveries about the molecular events involved in angiogenesis, and by developing a model specific to these experiments we are able to validate our predictions by direct comparison with the

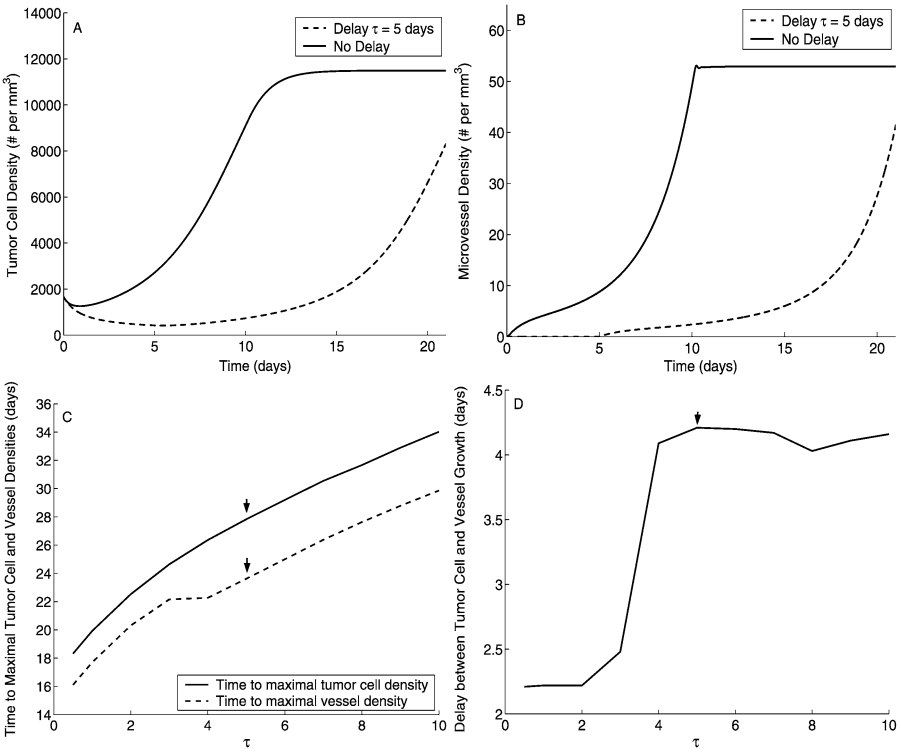

Fig. 8 Effect of the delay τ on tumor growth and vascular development. A, B, Comparison of tumor cell and vessel densities in the non-delay case ($\tau = 0$) versus the delay held at its baseline value ($\tau = 5$). The tumor cell density has already reached its maximal level by day 16 in the non-delay case (A). The vessel density reaches its maximal level by day 14 in the non-delay case, and are blood borne as soon as they are formed (B). C, D, As the delay is varied between biologically realistic values of 0.5 days to 10 days, the time taken to maximal tumor cell density increases by 89% while the time taken to reach maximal vessel density increases by about 88% (C). For τ between 0.5 and 3 days, the delay between tumor cell and vessel development is about 2 days, but for τ greater than 4 days, this delay increases to 4 days (D).

available data. It would be a straight forward task to change initial conditions to better describe traditional vascular tumor growth.

Numerical simulations of the full model provide insight into the growth dynamics of tumors with different sensitivities to oxygen deprivation and various rates of VEGF production. Results obtained showed that as tumors with increasing sensitivities to local oxygen concentration were considered, the time taken to reach maximum cell densities by the tumor increased, and tumor cell growth was significantly affected, but this had little impact on the vascular development of the tumor. Tumor cells highly sensitive to local oxygen concentrations were found to give rise to highly vascularized tumors, with very low tumor cell densities that were at just 7% of their values in tumors with very low local oxygen concentration sensitivity. The vessel densities in these two kinds of tumors did not differ significantly. VEGF production rate was found to have a more significant impact on the time taken to reach maximal cell and vessel densities. As VEGF production rate was decreased from a maximum by 87.5%, it took 264% more time for tumor cell density to

reach its maximal level and 335% more time for the vasculature to fully develop. These results suggested that possible anti-angiogenic therapies targeting VEGF may result in significant delays in tumor progression.

Since the discovery of tumor secreted angiogenesis factors, there has been considerable interest in developing anti-angiogenic therapies targeting these molecules. In particular, anti-VEGF treatment has proven relatively easy to develop in animal models, and has generally produced satisfactory results in terms of inhibiting tumor growth (Ferrara, 2002). Several of the anti-VEGF compounds that were efficacious in animal models are currently undergoing clinical trials (Cao, 2004). However, many of these compounds including angiostatin, endostatin, avastin, and matrix metalloproteinase inhibitors have produced disappointing results (Garber, 2002). Cao (2004) considers several possible reasons for this difficulty in replicating results from the animal models in humans. For instance, a late stage tumor may produce many more angiogenic factors than an early stage tumor, so that the efficacy of anti-VEGF treatment becomes crucially dependent on early detection. In addition, the treatment may not be effective if it relies on blocking intracellular signalling mediated by VEGF receptors, since there may exist other receptor-like molecules on an endothelial cell surface, that bind VEGF (such as neuropilin, which binds several VEGF isoforms) and thereby transduce pro-angiogenic signalling. Our model has a flexible framework in which these and other hypotheses can easily be tested. For instance, the molecular model described here can be modified to include equations describing additional angiogenic factors, and the anti-VEGF compounds mentioned above, and the efficacy of therapy can then be tested at various stages of tumor development. We also plan to mathematically and computationally investigate the effect of the small molecule inhibitor of VEGFR2, PTK787/ZK222584, which does not interfere with VEGF binding, though it does neutralize the intracellular signaling that VEGFR2 triggers in order to promote proliferation and survival. To test the robustness of our mathematical model, we will compare its capability to predict response to VEGFR2 therapeutic blockade with response to the blocking of VEGF itself.

The VEGF–Bcl-2–CXCL8 pathway also presented two new potential areas for the development of cancer treatment. Numerical results indicated that inhibiting the production of CXCL8 by HDMECs from day zero delayed the tumor progression, but did not affect the maximal tumor cell and vessel densities. The most promising strategy however was to block the up-regulation of Bcl-2 by VEGF in HDMECs, this resulted in a tumor with low vascular density and a correspondingly low tumor cell density. The tumor responded much better to treatment after a certain minimum level of therapy was applied. Anti Bcl-2 therapy significantly delayed tumor development as well. In a simulation carried out to test these two strategies on a fully developed tumor, we found that blocking CXCL8 production had virtually no effect on the tumor, but down regulation of Bcl-2 resulted in the tumor stabilizing at low cell and vessel densities. Hence, the dual role played by VEGF viz. enhanced endothelial cell survival due to up-regulation of Bcl-2 and increased endothelial cell proliferation and migration due to up-regulation of CXCL8 played a crucial role in the development of the tumor. Indeed, it appeared that increased endothelial cell half life was necessary for rapid growth and progression of the tumor. Finally, the effect of the delay parameter was investigated numerically, and it was observed that without any delay, the vasculature developed too rapidly. For the control value of the delay parameter, a time lag of 4 days was observed between tumor cell and vessel development.

For future work, we plan to investigate in greater detail the ability of our mathematical model to predict response to anti-CXCL8 treatment, as well as to differentiate the responses to inhibition of the ligand (i.e. CXCL8) from inhibition of its receptor (i.e. CXCR2). The ligand can be experimentally inhibited by polyclonal anti-human CXCL8 antibody and the receptor by polyclonal anti-human CXCR2 antibody. Further, Nör has demonstrated that small molecule inhibitors of Bcl-2 have a strong inhibitory effect on the angiogenic potential of endothelial cells (Nör et al., 2001a; Karl et al., 2005). It is not clear how the effect of small molecule inhibitors of Bcl2 compares with the effect of genetic inhibition of Bcl-2 with siRNA. We plan to make modifications to the mathematical modeling developed here in order to point out potential differences in response to inhibition of Bcl-2 with a drug delivered intravenously (small molecule inhibitor) or with a genetic strategy (siRNA-Bcl-2).

The mathematical model presented here consists of delay differential equations, and by keeping track of temporal changes in the tumor and endothelial cell densities, VEGF and CXCL8 concentrations and microvessel density, we have been able to study the potential of a number of possible cancer therapies targeted at the VEGF–Bcl-2–CXCL8 pathway. As the experimental data available are mostly density vs. time plots, this approach is the natural first choice. However, the vascular structure within a tumor is highly unorganized and spatially heterogeneous, and it would be instructive to extend this model to include spatial variations in cell densities, chemical concentrations and vascular development. A partial differential equation version of this model is also being developed which will include a discretized vessel equation, to enable us to track actual vessel movements.

Though we have concentrated on the downstream effects of VEGF, in reality, tumor-induced angiogenesis is a highly complex process involving several chemokines and proteins that participate in various cellular and sub-cellular events, and the full picture of these is still developing. For instance, basic fibroblast growth factor (bFGF) has been shown to be a potent mediator of angiogenesis, and in certain cancers, to increase the expression of Bcl-2 (Pepper et al., 1992; Ueno et al., 1997). Monocyte chemoattractant protein-1 (MCP-1) (Salcedo et al., 2000; Ohta et al., 2002) and growth related oncogene-alpha (groα) (Pepper et al., 1992) have been recently found to play a direct role in angiogenesis and tumor progression. We have also assumed that VEGF is produced by tumor cells alone, and CXCL8 is produced by free endothelial cells alone, while microvessel branching and maturation have been excluded. Further, other proteins with demonstrated influence on angiogenesis, such as angiopoietins and their Tie-2 receptor, which among other functions, are indicated in regulating vessel maturation, sprouting and regression (Bach et al., 2007) can easily be incorporated into this model and will likely be the subject of future work. To this end, we are in the process of extending this model to relax some of the above assumptions. This mathematical model together with the extensions mentioned above can provide a useful framework for enhancing the understanding of the interplay between mediators of tumor angiogenesis and for predicting the effectiveness of novel anti-angiogenic treatment strategies.

Acknowledgements

The authors thank the National Institute of Health Grant R01DE15948, which supported the experiments on which the paper is based. This research was supported by the Alfred P.

Sloan Foundation, and the James S. McDonnell foundation. The authors are also grateful to Elisabeta Karl (University of Michigan, Ann Arbor, MI) for providing experimental data in Fig. 6.

Appendix A: Full model equations

The full system of equations used to model sustained angiogenesis are given below.

$$\frac{dM}{dt} = \left(\mu_a \frac{D_a}{M+\alpha_1 V} + \mu_l \frac{C_l}{M+\alpha_1 V} - \left(\lambda_m - \delta \frac{D_a}{M+\alpha_1 V}\right)\right) \times M\left(1 - \frac{M}{M_0 - \alpha_1 V}\right) - \alpha_1\left(\alpha_2 \frac{D_a}{M+\alpha_1 V} + \alpha_3 \frac{C_l}{M+\alpha_1 V}\right) M_\tau, \tag{A.1}$$

$$\frac{dA}{dt} = -2\eta_1^a k_{f1}^a A R_a + \eta_2^a k_{r1}^a C_a - \lambda_a A + r_3 N\left(1 + \tanh\left(\frac{V_{\text{char}} - (V+V_0)}{\epsilon}\right)\right), \tag{A.2}$$

$$\frac{dR_a}{dt} = -2k_{f1}^a A R_a + \eta_3^a k_{r1}^a C_a - k_{f2}^a C_a R_a + 2\eta_4^a k_{r2}^a D_a + 2\eta_4^v k_p^a D_a, \tag{A.3}$$

$$\frac{dC_a}{dt} = 2\eta_5^a k_{f1}^a A R_a - k_{r1}^a C_a - \eta_5^a k_{f2}^a C_a R_a + 2\eta_6^a k_{r2}^a D_a, \tag{A.4}$$

$$\frac{dD_a}{dt} = \eta_7^a k_{f2}^a C_a R_a - 2k_{r2}^a D_a - k_p^a D_a, \tag{A.5}$$

$$\frac{dL}{dt} = -\eta_1^l k_f^l L R_l + \eta_2^l k_r^l C_l - \lambda_l L + \beta_l M + \beta_a \frac{D_a}{M+\alpha_1 V} M, \tag{A.6}$$

$$\frac{dR_l}{dt} = -k_f^l L R_l + \eta_3^l k_r^l C_l + \eta_3^l k_p^l C_l, \tag{A.7}$$

$$\frac{dC_l}{dt} = \eta_4^l k_f^l L R_l - k_r^l C_l - k_p^l C_l, \tag{A.8}$$

$$\frac{dV}{dt} = \left(\alpha_2 \frac{D_a}{M+\alpha_1 V} + \alpha_3 \frac{C_l}{M+\alpha_1 V}\right) M_\tau - \alpha_4\left(\lambda_m - \delta \frac{D_a}{M+\alpha_1 V}\right)\alpha_1 V, \tag{A.9}$$

$$\frac{dN}{dt} = r_1 \frac{C^2(V)}{C_1^2 + C^2(V)} N - r_2\left(1 - \sigma \frac{C^2(V)}{C_2^2 + C^2(V)}\right) N^2, \tag{A.10}$$

where

$$C(V) = C_m \frac{V_0 + V}{k + V_0 + V}. \tag{A.11}$$

Appendix B: Parameter values

Where possible, the choice of parameters is based on values given in the literature. In cases where no data could be found, parameter values were chosen so that endothelial cell

and microvessel densities best fit pre-treatment experimental data taken from Dong et al. (2007), Nör et al. (2001a, 1999). In each case, the model was first reduced to represent the in vitro or in vivo experimental system, then a least squares fit of the modified model to the HDMEC density or microvessel density vs. time experimental data was performed. Care was taken to fit no more than 2–3 parameters to any given set of experimental data. Biologically realistic values were chosen for the parameters for which no experimental data was available. All of the parameter estimation was done prior to simulation of treatment strategies, and these values were kept constant thereafter.

Table B.1 List of parameter values

Parameter	Value	Units	Source
μ_a	14.0875	# HDMECs per pg of D_a per day	Nör et al. (1999)[a]
μ_l	810.1032	# HDMECs per pg of C_l per day	Nör et al. (1999)[a]
λ_m	0.12	per day	Levine et al. (2001)
δ	21.56	# HDMECs per pg of D_a per day	Nör et al. (1999)[a]
α_1	30.0	# HDMECs per Microvessel	Levine et al. (2001), Norrby (1998), Ruhrberg et al. (2002)
α_2	0.2577	# Microvessels per pg of D_a per day	Dong et al. (2007)[a]
α_3	0.6741	# Microvessels per pg of C_l per day	Dong et al. (2007)[a]
M_0	17×10^3	# HDMECs per mm^3	Nör et al. (2001a)
k^a_{f1}	1.6232	per VEGF concentration per day	Mac Gabhann and Popel (2004), Wang et al. (2002)
k^a_{r1}	49.3025	per day	Mac Gabhann and Popel (2004), Wang et al. (2002)
k^a_{f2}	162.32	per C_a concentration per day	Mac Gabhann and Popel (2004), Wang et al. (2002)[b]
k^a_{r2}	0.493025	per day	Mac Gabhann and Popel (2004), Wang et al. (2002)[b]
k^a_p	16.0	per day	Wang et al. (2002)
η^a_1	0.2250	pg VEGF per pg R_a	Ferrara (1999), Stewart et al. (2003)
η^a_2	0.1837	pg VEGF per pg C_a	Ferrara (1999), Stewart et al. (2003)
η^a_3	0.8163	pg R_a per pg C_a	Ferrara (1999), Stewart et al. (2003)
η^a_4	0.4494	pg R_a per pg D_a	Ferrara (1999), Stewart et al. (2003)
η^a_5	1.2250	pg C_a per pg R_a	Ferrara (1999), Stewart et al. (2003)
η^a_6	0.5506	pg C_a per pg D_a	Ferrara (1999), Stewart et al. (2003)
η^a_7	2.2250	pg D_a per pg R_a	Ferrara (1999), Stewart et al. (2003)
λ_a	15.5958	per day	Serini et al. (2003)
r_3	0.0813	pg VEGF per Tumor cell per day	Nör et al. (2001a)[c]
V_{char}	55.0	# Microvessels per mm^3	[d]
V_0	2.0	# Microvessels per mm^3	[d]
ϵ	1.0	# Microvessels per mm^3	[d]
k^l_f	6.7587	per CXCL8 concentration per day	Nör et al. (1999)[a]

Table B.1 (*Continued*)

Parameter	Value	Units	Source
k_r^l	43.2557	per day	Holmes et al. (1991)
k_p^l	24.0	per day	Mukaida (2003)
η_1^l	0.1311	pg CXCL8 per pg R_l	Horuk (1994), Maher (1995), Samanta et al. (1989)
η_2^l	0.1159	pg CXCL8 per pg C_l	Horuk (1994), Maher (1995), Samanta et al. (1989)
η_3^l	0.8841	pg R_l per pg C_l	Horuk (1994), Maher (1995), Samanta et al. (1989)
η_4^l	1.1311	pg C_l per pg R_l	Horuk (1994), Maher (1995), Samanta et al. (1989)
λ^l	15.5958	per day	Serini et al. (2003)[e]
β_l	8.0924×10^{-4}	pg of CXCL8 per HDMEC per day	Nör et al. (1999)[a]
β_a	3.3766	pg of IL-8 per pg of D_a per day	Nör et al. (1999)[a]
α_4	0.24845	# Microvessels per HDMEC	Dong et al. (2007)[a]
r_1	1.2924	per day	Gammack and Byrne (2001)
C_1	0.1	Oxygen concentration	Gammack and Byrne (2001)
r_2	0.001	per Tumor cell density per day	Nör et al. (2001a)
σ	1.0029	dimensionless	Gammack and Byrne (2001)
C_2	0.054	Oxygen concentration	Gammack and Byrne (2001)
C_m	0.2	Oxygen concentration	Gammack and Byrne (2001)
k	8.0	# Microvessels per mm^3	[d]

[a]The parameters associated with CXCL8 and VEGF effect on HDMEC proliferation and death, and microvessel formation and degradation were estimated using least squares fits of experimental data in Nör et al. (1999) and Dong et al. (2007)

[b]It was assumed that the formation of a dimerized receptor-ligand (VEGFR2-VEGF) complex D_a proceeds forward at a much faster rate than the formation of a monomer receptor-ligand complex C_a, and that the dimerized complex is more stable than the monomer receptor-ligand complex

[c]Keeping all other parameter values fixed, VEGF production rate by tumor cells was determined by fitting the microvessel density after 21 days with that observed experimentally in a (control) tumor that was allowed to grow without the application of any anti-cancer therapy (Nör et al., 2001a)

[d]In the absence of experimental data, biologically realistic values for these parameters were chosen so that the solution profiles best fit experimental observations

[e]In the absence of experimental data, the half-life of CXCL8 was taken to be the same as that of VEGF for purposes of simplicity

References

Anderson, A.R., Chaplain, M.A., 1998. Continuous and discrete mathematical models of tumor-induced angiogenesis. Bull. Math. Biol. 60(5), 857–899.

Ausprunk, D.H., Folkman, J., 1977. Migration and proliferation of endothelial cells in preformed and newly formed blood vessels during tumor angiogenesis. Microvasc. Res. 14(1), 53–65.

Bach, F., Uddin, F.J., Burke, D., 2007. Angiopoietins in malignancy. Eur. J. Surg. Oncol. 33(1), 7–15.

Baxter, L.T., Jain, R.K., 1991. Transport of fluid and macromolecules in tumors. III. Role of binding and metabolism. Microvasc. Res. 41(1), 5–23.

Bernatchez, P.N., Soker, S., Sirois, M.G., 1999. Vascular endothelial growth factor effect on endothelial cell proliferation, migration, and platelet-activating factor synthesis is Flk-1-dependant. J. Biol. Chem. 274(43), 31047–31054.

Cao, Y., 2004. Antiangiogenic cancer therapy. Semin. Cancer Biol. 14(2), 139–145.

Chaplain, M.A., Anderson, A.R., 1996. Mathematical modelling, simulation and prediction of tumour-induced angiogenesis. Invasion Metastasis 16(4-5), 222–234.

Daugulis, P., Arakelyan, L., Ginosar, Y., Agur, Z., 2004. Hopf point analysis for angiogenesis models. Discret. Contin. Dyn. Syst. Ser. B 4(1), 29–38.

Dong, Z., Song, W., Sun, Q., Zeitlin, B.D., Karl, E., Spencer, D.M., Jain, H.V., Jackson, T., Núñez, G., Nör, J.E., 2007. Endothelial cell apoptosis and microvessel disruption. Exp. Cell Res., accepted.

Dvorak, H.F., Brown, L.F., Detmar, M., Dvorak, A.M., 1995. Vascular permeability factor/vascular endothelial growth factor, vascular hyperpermeability, and angiogenesis. Am. J. Pathol. 146(5), 1029–1039.

Ferrara, N., 1999. Molecular and biological properties of vascular endothelial growth factor. J. Mol. Med. 77(7), 527–543.

Ferrara, N., 2002. VEGF and the quest for tumour angiogenesis factors. Nat. Rev. Cancer 2, 795–803.

Ferrara, N., Gerber, H.P., LeCouter, J., 2003. The biology of VEGF and its receptors. Nat. Med. 9(6), 669–676.

Folkman, J., 1971. Tumor angiogenesis: therapeutic implications. N. Engl. J. Med. 285(21), 1182–1186.

Gammack, D., Byrne, H.M., 2001. Estimating the selective advantage of mutant p53 tumour cells to repeated rounds of hypoxia. Bull. Math. Biol. 63(1), 135–166.

Garber, K., 2002. Angiogenesis inhibitors suffer new setback. Nat. Biotechnol. 20, 1067–1068.

Gille, H., Kowalski, J., Li, B., LeCouter, J., Moffat, B., Zioncheck, T.F., Pelletier, N., Ferrara, N., 2001. Analysis of biological effects and signaling properties of Flt-1 (VEGFR-1) and KDR (VEGFR-2). A reassessment using novel receptor-specific vascular endothelial growth factor mutants. J. Biol. Chem. 276(5), 3222–3230.

Guglielmi, N., Hairer, E., 2001. Implementing Radau IIA methods for stiff delay differential equations. Computing 67(1), 1–12.

Holmes, M.J., Sleeman, B.D., 2000. A mathematical model of tumour angiogenesis incorporating cellular traction and viscoelastic effects. J. Theor. Biol. 202(2), 95–112.

Holmes, W.E., Lee, J., Kuang, W.J., Rice, G.C., Wood, W.I., 1991. Structure and functional expression of a human interleukin-8 receptor. Science 253(5025), 1278–1280.

Horuk, R., 1994. The interleukin-8-receptor family: from chemokines to malaria. Immunol. Today 15(4), 169–174.

Karl, E., Warner, K., Zeitlin, B., Kaneko, T., Wurtzel, L., Jin, T., Chang, J., Wang, S., Wang, C.Y., Strieter, R.M., Nunez, G., Polverini, P.J., Nör, J.E., 2005. Bcl-2 acts in a proangiogenic signaling pathway through nuclear factor-kappaB and CXC chemokines. Cancer Res. 65(12), 5063–5069.

Ke, L.D., Shi, Y.X., Im, S.A., Chen, X., Yung, W.K., 2000. The relevance of cell proliferation, vascular endothelial growth factor, and basic fibroblast growth factor production to angiogenesis and tumorigenicity in human glioma cell lines. Clin. Cancer Res. 6(6), 2562–2572.

Kim, K.J., Li, B., Winer, J., Armanini, M., Gillett, N., Phillips, H.S., Ferrara, N., 1993. Inhibition of vascular endothelial growth factor-induced angiogenesis suppresses tumour growth in vivo. Nature 362(6423), 841–844.

Klintworth, G.K., 1973. The hamster cheek pouch: an experimental model of corneal vascularization. Am. J. Pathol. 73(3), 691–710.

Koch, A.E., Polverini, P.J., Kunkel, S.L., Harlow, L.A., DiPietro, L.A., Elner, V.M., Elner, S.G., Strieter, R.M., 1992. Interleukin-8 as a macrophage-derived mediator of angiogenesis. Science 258(5089), 1798–1801.

Kuang, Y., Nagy, J.D., Elser, J.J., 2004. Biological stoichiometry of tumor dynamics. Discret. Contin. Dyn. Syst. Ser. B 4(1), 221–240.

Leung, D.W., Cachianes, G., Kuang, W.J., Goeddel, D.V., Ferrara, N., 1989. Vascular endothelial growth factor is a secreted angiogenic mitogen. Science 246(4935), 1306–1309.

Levine, H.A., Sleeman, B.D., Nilsen-Hamilton, M., 2000. A mathematical model for the roles of pericytes and macrophages in the initiation of angiogenesis. I. The role of protease inhibitors in preventing angiogenesis. Math. Biosci. 168(1), 77–115.

Levine, H.A., Pamuk, S., Sleeman, B.D., Nilsen-Hamilton, M., 2001. Mathematical modeling of capillary formation and development in tumor angiogenesis: penetration into the stroma. Bull. Math. Biol. 63(5), 801–863.

Levine, H.A., Tucker, A.L., Nilsen-Hamilton, M., 2002. A mathematical model for the role of cell signal transduction in the initiation and inhibition of angiogenesis. Growth Factors 20(4), 155–175.

Mac Gabhann, F., Popel, A.S., 2004. Model of competitive binding of vascular endothelial growth factor and placental growth factor to VEGF receptors on endothelial cells. Am. J. Physiol. Heart Circ. Physiol. 286(1), H153–H164.

McMahon, G., 2000. VEGF receptor signalling in tumor angiogenesis. Oncologist 5, 3–10.

Maher, J.J., 1995. Rat hepatocytes and Kupffer cells interact to produce interleukin-8 (CINC) in the setting of ethanol. Am. J. Physiol. 269(4 Pt 1), G518–G523.
Mukaida, N., 2003. Pathophysiological roles of interleukin-8/CXCL8 in pulmonary diseases. Am. J. Physiol. Lung Cell. Mol. Physiol. 284(4), L566–L577.
Nagy, J.D., 2004. Competition and natural selection in a mathematical model of cancer. Bull. Math. Biol. 66(4), 663–687.
Nguyen, M., Shing, Y., Folkman, J., 1994. Quantitation of angiogenesis and antiangiogenesis in the chick embryo chorioallantoic membrane. Microvasc. Res. 47(1), 31–40.
Nör, J.E., Christensen, J., Mooney, D.J., Polverini, P.J., 1999. Vascular endothelial growth factor (VEGF)-mediated angiogenesis is associated with enhanced endothelial cell survival and induction of Bcl-2 expression. Am. J. Pathol. 154(2), 375–384.
Nör, J.E., Christensen, J., Liu, J., Peters, M., Mooney, D.J., Strieter, R.M., Polverini, P.J., 2001a. Up-Regulation of Bcl-2 in microvascular endothelial cells enhances intratumoral angiogenesis and accelerates tumor growth. Cancer Res. 61(5), 2183–2188.
Nör, J.E., Peters, M.C., Christensen, J.B., Sutorik, M.M., Linn, S., Khan, M.K., Addison, C.L., Mooney, D.J., Polverini, P.J., 2001b. Engineering and characterization of functional human microvessels in immunodeficient mice. Lab. Invest. 81(4), 453–463.
Norrby, K., 1998. Microvascular density in terms of number and length of microvessel segments per unit tissue volume in mammalian angiogenesis. Microvasc. Res. 55(1), 43–53.
Ohta, M., Kitadai, Y., Tanaka, S., Yoshihara, M., Yasui, W., Mukaida, N., Haruma, K., Chayama, K., 2002. Monocyte chemoattractant protein-1 expression correlates with macrophage infiltration and tumor vascularity in human esophageal squamous cell carcinomas. Int. J. Cancer 102(3), 220–224.
Oikawa, T., Sasaki, M., Inose, M., 1997. Effect of cytogenin, a novel microbial product, on embryonic and tumor cell induced angiogenic responses in vivo. Anticancer Res. 17(3C), 1881–1886.
Patan, S., 2000. Vasculogenesis and angiogenesis as mechanisms of vascular network formation, growth and remodeling. J. Neurooncol. 50(1–2), 1–15.
Pepper, M.S., Ferrara, N., Orci, L., Montesano, R., 1992. Potent synergism between vascular endothelial growth factor and basic fibroblast growth factor in the induction of angiogenesis in vitro. Biochem. Biophys. Res. Commun. 189(2), 824–831.
Pettet, G.J., Byrne, H.M., McElwain, D.L., Norbury, J., 1996a. A model of wound-healing angiogenesis in soft tissue. Math. Biosci. 136(1), 35–63.
Pettet, G., Chaplain, M.A., McElwain, D.L., Byrne, H.M., 1996b. On the role of angiogenesis in wound healing. Proc. Biol. Sci. 263(1376), 1487–1493.
Plank, M.J., Sleeman, B.D., 2003. A reinforced random walk model of tumour angiogenesis and anti-angiogenic strategies. Math. Med. Biol. 20(2), 135–181.
Plank, M.J., Sleeman, B.D., Jones, P.F., 2004. A mathematical model of tumour angiogenesis, regulated by vascular endothelial growth factor and the angiopoietins. J. Theor. Biol. 229(4), 435–454.
Pradeep, C.R., Sunila, E.S., Kuttan, G., 2005. Expression of vascular endothelial growth factor (VEGF) and VEGF receptors in tumor angiogenesis and malignancies. Integr. Cancer Ther. 4(4), 315–321.
Ribatti, D., Vacca, A., Roncali, L., Dammacco, F., 1996. The chick embryo chorioallantoic membrane as a model for in vivo research on angiogenesis. Int. J. Dev. Biol. 40(6), 1189–1197.
Ruhrberg, C., Gerhardt, H., Golding, M., Watson, R., Ioannidou, S., Fujisawa, H., Betsholtz, C., Shima, D.T., 2002. Spatially restricted patterning cues provided by heparin-binding VEGF-A control blood vessel branching morphogenesis. Genes Dev. 16(20), 2684–2698.
Salcedo, R., Ponce, M.L., Young, H.A., Wasserman, K., Ward, J.M., Kleinman, H.K., Oppenheim, J.J., Murphy, W.J., 2000. Human endothelial cells express CCR2 and respond to MCP-1: direct role of MCP-1 in angiogenesis and tumor progression. Blood 96(1), 34–40.
Samanta, A.K., Oppenheim, J.J., Matsushima, K., 1989. Identification and characterization of specific receptors for monocyte-derived neutrophil chemotactic factor (MDNCF) on human neutrophils. J. Exp. Med. 169(3), 1185–1189.
Serini, G., Ambrosi, D., Giraudo, E., Gamba, A., Preziosi, L., Bussolino, F., 2003. Modeling the early stages of vascular network assembly. EMBO J. 22(8), 1771–1779.
Shweiki, D., Neeman, M., Itin, A., Keshet, E., 1995. Induction of vascular endothelial growth factor expression by hypoxia and by glucose deficiency in multicell spheroids: Implications for tumor angiogenesis. Proc. Natl. Acad. Sci. USA 92(3), 768–772.
Siemeister, G., Schirner, M., Reusch, P., Barleon, B., Marme, D., Martiny-Baron, G., 1998. An antagonistic vascular endothelial growth factor (VEGF) variant inhibits VEGF-stimulated receptor autophosphorylation and proliferation of human endothelial cells. Proc. Natl. Acad. Sci. USA 95(8), 4625–4629.

Smith, D.R., Polverini, P.J., Kunkel, S.L., Orringer, M.B., Whyte, R.I., Burdick, M.D., Wilke, C.A., Strieter, R.M., 1994. Inhibition of interleukin 8 attenuates angiogenesis in bronchogenic carcinoma. J. Exp. Med. 179(5), 1409–1415.

Spyridopoulos, I., Brogi, E., Kearney, M., Sullivan, A.B., Cetrulo, C., Isner, J.M., Losordo, D.W., 1997. Vascular endothelial growth factor inhibits endothelial cell apoptosis induced by tumor necrosis factor-alpha: balance between growth and death signals. J. Mol. Cell. Cardiol. 29(5), 1321–1330.

Stewart, M., Turley, H., Cook, N., Pezzella, F., Pillai, G., Ogilvie, D., Cartlidge, S., Paterson, D., Copley, C., Kendrew, J., Barnes, C., Harris, A.L., Gatter, K.C., 2003. The angiogenic receptor KDR is widely distributed in human tissues and tumours and relocates intracellularly on phosphorylation. An immunohistochemical study. Histopathology 43(1), 33–39.

Strieter, R.M., Kunkel, S.L., Elner, V.M., Martonyi, C.L., Koch, A.E., Polverini, P.J., Elner, S.G., 1992. Interleukin-8. A corneal factor that induces neovascularization. Am. J. Pathol. 141(6), 1279–1284.

Tee, D., DiStefano, J., 2004. Simulation of tumor-induced angiogenesis and its response to anti-angiogenic drug treatment: mode of drug delivery and clearance rate dependencies. J. Cancer Res. Clinical Oncol. 130(1), 15–24.

Terranova, V.P., DiFlorio, R., Lyall, R.M., Hic, S., Friesel, R., Maciag, T., 1985. Human endothelial cells are chemotactic to endothelial cell growth factor and heparin. J. Cell. Biol. 101(6), 2330–2334.

Trettel, F., Di Bartolomeo, S., Lauro, C., Catalano, M., Ciotti, M.T., Limatola, C., 2003. Ligand-independent CXCR2 dimerization. J. Biol. Chem. 278(42), 40980–40988.

Ueno, H., Li, J.J., Masuda, S., Qi, Z., Yamamoto, H., Takeshita, A., 1997. Adenovirus-mediated expression of the secreted form of basic fibroblast growth factor (FGF-2) induces cellular proliferation and angiogenesis in vivo. Arterioscler. Thromb. Vasc. Biol. 17(11), 2453–2460.

Wang, D., Lehman, R.E., Donner, D.B., Matli, M.R., Warren, R.S., Welton, M.L., 2002. Expression and endocytosis of VEGF and its receptors in human colonic vascular endothelial cells. Am. J. Physiol. Gastrointest. Liver Physiol. 282(6), G1088–G1096.

Ward, J.P., King, J.R., 1999. Mathematical modelling of avascular-tumour growth. II: Modelling growth saturation. IMA J. Math. Appl. Med. Biol. 16(2), 171–211.

Wilson, S., Wilkinson, G., Milligan, G., 2005. The CXCR1 and CXCR2 receptors form constitutive homo- and heterodimers selectively and with equal apparent affinities. J. Biol. Chem. 280(31), 28663–28674.

Yonekura, K., Basaki, Y., Chikahisa, L., 1999. UFT and its metabolites inhibit the angiogenesis induced by murine renal cell carcinoma, as determined by a dorsal air sac assay in mice. Clin. Cancer Res. 5(8), 2185–2191.